An Improved Liquid Water Absorption Model at Microwave Frequencies for Supercooled Liquid Water Clouds

D. D. TURNER

NOAA/National Severe Storms Laboratory, Norman, Oklahoma

S. KNEIFEL

Department of Atmospheric and Oceanic Sciences, McGill University, Montreal, Quebec, Canada

M. P. CADEDDU

Argonne National Laboratory, Lemont, Illinois

(Manuscript received 15 April 2015, in final form 10 September 2015)

ABSTRACT

An improved liquid water absorption model is developed for frequencies between 0.5 and 500 GHz. The empirical coefficients for this model were retrieved from a dataset that consists of both laboratory observations of the permittivity of liquid water (primarily at temperatures above 0°C) and field observations collected by microwave radiometers in three separate locations with observations at temperatures as low as −32°C. An optimal estimation framework is used to retrieve the model's coefficients. This framework shows that there is high information content in the observations for seven of the nine model coefficients, but that the uncertainties in all of the coefficients result in less than 15% uncertainty in the liquid water absorption coefficient for all temperatures between −32° and 0°C and frequencies between 23 and 225 GHz. Furthermore, this model is more consistent with both the laboratory and field observations over all frequencies and temperatures than other popular absorption models.

1. Introduction

Supercooled water clouds that contain liquid water at temperatures below 0°C are a common occurrence around the globe (Hogan et al. 2004; Hu et al. 2010). To understand their role in the weather/climate system, accurate measurements of their macrophysical and microphysical properties are needed. One of the most basic properties is the vertically integrated liquid water content, which is referred to as the liquid water path (LWP). LWP can be retrieved from cloud radar (e.g., Matrosov et al. 2004), visible/near-infrared radiances (e.g., Minnis et al. 1995; Greenwald 2009; Heng et al. 2014), and thermal infrared radiance observations (e.g., Turner 2007), but the most common retrieval methods use microwave and submillimeter wave radiometer observations (e.g., Curry et al. 1990; Petty and Katsaros 1992; Lin and Rossow 1994; Westwater et al. 2001; Turner et al. 2007; Greenwald et al. 1993; O'Dell et al. 2008).

However, retrievals of LWP from satellite- and ground-based radiometer observations require that the underlying radiative transfer model used in the retrieval is accurate and does not suffer from systematic biases. In the microwave and submillimeter wave portion of the spectrum from roughly 0.5 to 300 GHz (henceforth referred to as the microwave for simplicity), the dielectric properties (i.e., refractive indices) of liquid water (and therefore its interaction with radiation) are temperature dependent. Historically, the temperature dependence of the refractive index has been measured in the laboratory, and as a result of a range of technical issues, the measurements have largely been at temperatures above 0°C. Many semiempirical models were fit to the laboratory data and used to extrapolate the laboratory-measured absorption to supercooled temperatures. However, several papers (e.g., Westwater et al. 2001; Lin et al. 2001; Ellison 2007; Kneifel et al. 2014) have illustrated that

Corresponding author address: D. D. Turner, Physical Scientist, NOAA/National Severe Storms Laboratory, 120 David L. Boren Blvd., Norman, OK 73072.
E-mail: dave.turner@noaa.gov

DOI: 10.1175/JTECH-D-15-0074.1

there are significant differences in the absorption coefficients predicted by these models at low temperatures (e.g., −20°C). These differences in the absorption coefficients translate directly into errors in the retrieved LWP, potentially as large as 50% or more depending on the frequencies and the temperature of the cloud (Kneifel et al. 2014, hereafter Kneifel14).

Cloud droplets are very small relative to the wavelength of radiation in the microwave region of the spectrum, and thus the Rayleigh approximation can be used to calculate the mass absorption coefficient. This coefficient, α_L, is a function of frequency ν of the radiation field and is computed as

$$\alpha_L = \frac{6\pi\nu}{\rho_L c}\,\mathrm{Im}\left(\frac{\varepsilon - 1}{\varepsilon + 2}\right), \tag{1}$$

where ρ_L is the density of the liquid water, c is the speed of light in a vacuum, $\varepsilon = \varepsilon' + i\varepsilon''$ is the complex dielectric permittivity of the liquid water, and $\mathrm{Im}(x)$ is the imaginary part of the complex number x. Most liquid water absorption models in the microwave spectral region actually predict the complex permittivity ε using various formulations of the Debye model (Debye 1929); empirically determined coefficients are used with the model to interpolate laboratory observations that were made at a small number of frequencies and temperatures to other frequencies and temperatures. Ellison (2007, hereafter Ellison07) and Kneifel14 provide detailed discussions of the differences among different absorption models used by the community. However, the key point is that all of these models use empirically determined coefficients to fit their assumed model to the data and to interpolate to the desired temperature and frequency.

Here, we have refit the empirical coefficients of one of the more recent liquid water absorption models using both the laboratory data used in the original fitting together with new field data that include observations of liquid water down to temperatures below −30°C. The datasets used in the analysis and the model we have elected to refit will be discussed, and the methodology used to determine the new model coefficients will be described. Our fitting method provides a quantitative estimate of the number of independent pieces of information in the data, as well as a full error covariance matrix that will be used to provide uncertainty estimates in the absorption coefficients that are derived from the new absorption model.

2. Datasets

a. Laboratory data

Laboratory measurements of the absorption properties of liquid water in the microwave portion of the spectrum have been made for over a century, with some of the first quantitative measurements being made in the late 1880s (e.g., Tereschin 1889). A detailed historical review of the laboratory measurements of the dielectric permittivity of liquid water (ε) is given in Ellison et al. (1996, hereafter Ellison96). Ellison and his coauthors did a tremendous service for the community by carefully scrutinizing over 60 published laboratory datasets, evaluating the methods used and presenting the results in order to attempt to assign an uncertainty estimate for each, and then compiling all of this information into an easy-to-use table.

Many of these laboratory studies focused on either a single frequency and made observations over two or more temperatures or made observations at several frequencies at a single temperature. As our purpose is to improve the accuracy of liquid water dielectric models for use in quantifying absorption in the earth's atmosphere, we chose only laboratory data collected at temperatures below 50°C. Furthermore, since the focus is on improving liquid water path retrievals from microwave radiometers, the laboratory data were also restricted to frequencies smaller than 500 GHz (the channels of virtually all microwave radiometers that are used for remote sensing are below this frequency). The full references and description of these data can be found in Ellison96.

There are 1130 points in our selected laboratory dataset. The frequencies in this selected dataset range from 0.465 to 480 GHz, with the median frequency at 9.4 GHz and the 25th and 75th percentiles of 4.1 and 23.8 GHz, respectively. The temperatures in this dataset range from −18.2° to 50.0°C, with a median temperature of 25.0°C and the 25th and 75th percentile values of 15.0° and 30.0°C, respectively. Note that there are only six laboratory observations at temperatures below −5°C; these observations were made by Bertolini et al. (1982) at a single frequency (9.61 GHz). Most of these measurements were made at temperatures above 0°C owing to the difficulty of keeping supercooled liquid water from freezing in the laboratory.

The uncertainties in the above-mentioned data, as estimated by Ellison96, range from as low as 0.15% to over 150%. We felt that the extremely small relative uncertainties were unrealistic, and to evaluate this, we applied our fitting methodology (explained in section 4) to these laboratory data to refit the Ellison07 model. We were only able to produce a fit similar to the Ellison07 model if we assumed that the uncertainty in the laboratory measurements was 5% or the value specified by Ellison96, whichever was larger. Thus, these are the

uncertainty values that we applied to the laboratory data in the fitting of our new model (described below).

b. Field data

The field observations used in this study, which were compiled by Kneifel14, were collected at three sites: a low-altitude (511 m MSL) mountainous site in southwest Germany (Wulfmeyer et al. 2008), a site in the German Alps at 2650 m MSL (Löhnert et al. 2011), and a very cold and dry site in the center of Greenland (3250 m MSL; Shupe et al. 2013). Observations at 31.4, 52.28, 90, and 150 GHz were collected at all three sites, and observations at 225 GHz were also collected at the Greenland site. All of the radiometers used in this study were built by the same manufacturer and used the same technique to stabilize the temperature of the radiometric components of the microwave radiometers to ensure stable operations (Rose et al. 2005). The radiometers that collected these observations were calibrated using both tip-curve calibrations (e.g., Han and Westwater 2000) and liquid nitrogen as a cold reference target (e.g., Maschwitz et al. 2013). Additional details of the sites and microwave radiometers can be found in Kneifel14.

Microwave radiometers measure downwelling radiance, which is a function of the total opacity of the atmosphere, and thus it is a technique that is needed to separate out the contribution from liquid water absorption from that associated with water vapor, oxygen, and other absorbing gases. Kneifel14 use ratios of the opacity observed at different frequencies (e.g., 31.4 and 90 GHz), as suggested by Mätzler et al. (2010), to identify the liquid water contribution because cloud liquid water concentration changes much faster temporally than changes in the concentration of atmospheric gases. At any given ν, the fast changes in the opacity at that wavelength are related to fast changes in the LWP as

$$\Delta\tau_L(\nu, T_{\text{cld}}) = \Delta\text{LWP}\alpha_L(\nu, T_{\text{cld}}) \tag{2}$$

and thus the opacity ratio of frequencies ν_x and ν_y simplifies to

$$\gamma_{\nu_x,\nu_y}(T_{\text{cld}}) = \frac{\alpha_L(\nu_x, T_{\text{cld}})}{\alpha_L(\nu_y, T_{\text{cld}})}. \tag{3}$$

Note that there is no LWP dependence in Eq. (3). Kneifel14 demonstrated that the opacity ratios for different frequency combinations were very consistent from site to site, and that the observations from all three sites spanned the supercooled temperature range from 0° to −32°C. Kneifel14 combined ceilometer and cloud radar observations to determine cloud boundaries. Radiosonde data (from the low-altitude and Greenland sites) or numerical weather prediction analysis data (from the site in the Alps) were used together with the cloud boundaries to derive the temperature of the cloud (T_{cld}) and to estimate its uncertainty; additional details are described in Kneifel14.

To use the field data in this study, the opacity ratios of pairs of frequencies needed to be converted into a dataset of liquid water absorption coefficients α_L at the different frequencies. To do this, we followed the approach used by Kneifel14, wherein a reference model for $\alpha_{L,\text{ref}}(\nu_{\text{ref}}, T_{\text{cld}})$ over the entire supercooled temperature range was used to compute $\alpha_L(\nu_x, T_{\text{cld}})$ from any other frequency ν_x using the observed $\gamma_{\nu_x,\nu_y}(T_{\text{cld}})$ and Eq. (3). Mätzler et al. (2010) and Cadeddu and Turner (2011) independently showed that the model of Stogryn et al. (1995, hereafter Stogryn95) matched observations of α_L well at 90 GHz. Thus, this model at 90 GHz was used as the reference in order to compute α_L at the other frequencies from the opacity ratio data.

To account for uncertainty in the Stogryn95 model, we assumed that the error is 10% at 0°C and increases to 30% at −30°C, based on the previously mentioned studies. These errors were combined with the observational uncertainties in $\gamma_{\nu_x,\nu_y}(T_{\text{cld}})$ to provide the uncertainty in these field observations at each wavelength and temperature bin.

3. Model background

The dielectric permittivity of a material describes how that substance interacts with an electromagnetic field. It depends strongly on the molecular structure of the matter itself and is often a function of wavelength, temperature, and pressure. For pure liquid water, the effect of variations in pressure on the dielectic permittivity is relatively small, and thus virtually all liquid water absorption models are concerned with predicting permittivity as a function of frequency and temperature, that is, $\varepsilon(\nu, T)$.

A wide variety of different interpolation functions has been fit to laboratory observations and used to predict ε. Many absorption models, such as Ellison07, Stogryn95, and Liebe et al. (1991, hereafter Liebe91), used a "double Debye" model to fit the observed laboratory data for frequencies less than 500 GHz. The primary challenge for these previous models is the lack of liquid water absorption observations for supercooled temperatures, and thus all of these models extrapolate to temperatures lower than 0°C. However, the recent model of Rosenkranz (2015, hereafter Rosenkranz15), which uses the Kneifel14 data as part of its development, uses a functional form that is different from the double-Debye model employed by others.

The single or multiple Debye formulations (depending on the number of terms in the summations) for the real and imaginary permittivity coefficients are

$$\varepsilon' = \varepsilon_s - (2\pi\nu)^2 \sum_i A_i \tag{4}$$

and

$$\varepsilon'' = (2\pi\nu) \sum_i B_i, \tag{5}$$

respectively, where ε_s is the static dielectric constant. The static dielectric constant has been fit empirically with excellent precision (Hamelin et al. 1998) as

$$\varepsilon_s = s_0 + s_1 T + s_2 T^2 + s_3 T^3, \tag{6}$$

where T is the temperature of the liquid (°C) and the coefficients s_0, s_1, s_2, and s_3 were determined to be 8.7914×10^{1}, $-4.0440 \times 10^{-1}\,°C^{-1}$, $9.5873 \times 10^{-4}\,°C^{-2}$, and $-1.3280 \times 10^{-6}\,°C^{-3}$, respectively. Meissner and Wentz (2004) demonstrated that different models of ε_s, which were fit to observations, deviated less than 0.03% over the temperature range between −20° and +40°C.

The summation terms on the right-hand sides of Eqs. (4) and (5) contain the relaxation terms associated with this model. Because a double-Debye model was assumed, there are two terms in each summation. The form of these relaxation terms is given by

$$A_i = \frac{\tau_i^2 \Delta_i}{1 + (2\pi\nu\tau_i)^2} \tag{7}$$

and

$$B_i = \frac{\tau_i \Delta_i}{1 + (2\pi\nu\tau_i)^2}, \tag{8}$$

respectively, where

$$\Delta_i = a_i \exp(-b_i T) \tag{9}$$

and

$$\tau_i = c_i \exp\left(\frac{d_i}{T + t_c}\right). \tag{10}$$

Thus, for a double-Debye model, there are nine free parameters that are fit to the observations: a_1, b_1, c_1, and d_1 for the first Debye term; a_2, b_2, c_2, and d_2 for the second Debye term; and the "critical" temperature t_c, which should be close to the glass transition temperature of pure water (Ellison07). In these calculations, the frequency ν is in hertz.

TABLE 1. The coefficients for the double-Debye model of Ellison07 and TKC, the 1σ uncertainty in the TKC coefficients, the difference in the coefficients between the two models (%), and the DFS for each coefficient from the TKC fitting process. The total DFS was 7.0 out of a total possible of 9.

Coef	Ellison07	TKC	1σ in TKC	Diff	DFS
a_1	$7.942 \times 10^{+1}$	$8.111 \times 10^{+1}$	2.560×10^{-1}	2.1	1.00
b_1	4.320×10^{-3}	4.434×10^{-3}	8.760×10^{-5}	2.6	0.99
c_1	1.353×10^{-13}	1.302×10^{-13}	7.873×10^{-15}	−3.8	0.95
d_1	$6.533 \times 10^{+2}$	$6.627 \times 10^{+2}$	$1.619 \times 10^{+1}$	1.4	0.99
a_2	$3.612 \times 10^{+0}$	$2.025 \times 10^{+0}$	2.954×10^{-1}	−43.9	0.89
b_2	1.231×10^{-2}	1.073×10^{-2}	2.868×10^{-3}	−12.9	0.13
c_2	1.005×10^{-14}	1.012×10^{-14}	2.455×10^{-15}	−0.6	0.05
d_2	$7.431 \times 10^{+2}$	$6.089 \times 10^{+2}$	$3.595 \times 10^{+1}$	−18.1	0.96
t_c	$1.326 \times 10^{+2}$	$1.342 \times 10^{+2}$	$1.828 \times 10^{+0}$	1.2	1.00

After the nine empirical coefficients are determined for the desired temperature and frequency, the liquid water absorption is computed using Eq. (1).

4. Fitting methodology

Since all models of liquid water absorption in the microwave are semiempirical, we wanted to use a technique that would provide both the uncertainties in the derived absorption coefficients and the information content used in the fitting procedure for each of the empirical coefficients. We elected to use the so-called optimal estimation framework (Rodgers 2000), which is an iterative Gauss–Newton retrieval technique, to derive the empirical coefficients (represented by the vector $\mathbf{X}$). The objective of this study was to derive the optimal value of $\mathbf{X}$, as well as the uncertainty in $\mathbf{X}$ as specified by the posterior covariance matrix $\mathbf{S_X}$.

A Bayesian approach like the optimal estimation framework requires prior information ($\mathbf{X}_a$), which is used to constrain the solution and serve as the initial first guess. Here, the coefficients determined by Ellison07 were used as $\mathbf{X}_a$ (Table 1). To specify the error covariance of the prior ($\mathbf{S}_a$), we assume that there was a 25% uncertainty in each of these coefficients and that the errors are uncorrelated; this results in a diagonal matrix (note that assuming 100% uncertainty in $\mathbf{S}_a$ did not change the results given below significantly, as will be discussed in section 5).

The forward model (F) is Ellison07's formulation of the double-Debye model (section 3). The observational vector ($\mathbf{Y}$) is constructed to contain both the field and laboratory observations (section 2; Turner 2015), and the uncertainties are assumed to be uncorrelated and are used to specify the observational covariance matrix $\mathbf{S_Y}$.

Starting with the first guess, the framework was iterated to provide an improved value of $\mathbf{X}^{n+1}$ using the formulation

$$\mathbf{X}^{n+1} = \mathbf{X}_a + \mathbf{S}\mathbf{K}_n^T\mathbf{S}_\mathbf{Y}^{-1}[\mathbf{Y} - F(\mathbf{X}^n) + \mathbf{K}_n(\mathbf{X}^n - \mathbf{X}_a)], \quad (11)$$

where $\mathbf{K}_n$ is the Jacobian of F computed at $\mathbf{X}^n$, and T and superscript -1 denote the matrix operations transpose and inverse, respectively. The forward model F is a combination of Eqs. (4), (5), and (1) (depending on whether the observational element in $\mathbf{Y}$ is one of the laboratory measurements of permittivity or the field measurement of absorption). The error covariance of the solution $\mathbf{S}$ is given by

$$\mathbf{S} = (\mathbf{S}_a^{-1} + \mathbf{K}_n^T\mathbf{S}_\mathbf{Y}^{-1}\mathbf{K}_n)^{-1}. \quad (12)$$

The retrieval is iterated until

$$(\mathbf{X}^n - \mathbf{X}^{n+1})^T\mathbf{S}^{-1}(\mathbf{X}^n - \mathbf{X}^{n+1}) \ll N, \quad (13)$$

where $N = 9$ (i.e., the dimension of the vector $\mathbf{X}$). In this study, the threshold for convergence is 1.8 (i.e., 5 times smaller than N).

This framework required three iterations before the convergence criteria given in Eq. (13) was met. The coefficients for this new Turner–Kneifel–Cadeddu (TKC) model, along with the 1σ uncertainties in the TKC coefficients that come directly from the matrix $\mathbf{S}$ on the final iteration, are provided in Table 1. The relative changes between the Ellison07 coefficients and the new TKC coefficients are show in Fig. 1a and Table 1, and the uncertainties in the latter in Fig. 1b.

One important question is simply, Is there enough information in the laboratory and field observations to fit all nine coefficients used in the TKC model, and what is the information content for each coefficient? This can be answered by considering the degrees of freedom for signal (DFS), which is easily derived from the optimal estimation framework (Rodgers 2000). The diagonal of the averaging kernel $\mathbf{A}$ provides the DFS for each coefficient, where $\mathbf{A}$ is computed as

$$\mathbf{A} = \mathbf{S}\mathbf{K}_n^T\mathbf{S}_\mathbf{Y}^{-1}\mathbf{K}_n. \quad (14)$$

Rearranging Eq. (12) gives

$$\mathbf{K}_n^T\mathbf{S}_\mathbf{Y}^{-1}\mathbf{K}_n = \mathbf{S}^{-1} - \mathbf{S}_a^{-1} \quad (15)$$

and multiplying both sides of Eq. (15) by $\mathbf{S}$ yields

$$\mathbf{A} = \mathbf{S}\mathbf{K}_n^T\mathbf{S}_\mathbf{Y}^{-1}\mathbf{K}_n = \mathbf{S}(\mathbf{S}^{-1} - \mathbf{S}_a^{-1}) = \mathbf{I} - \mathbf{S}\mathbf{S}_a^{-1}. \quad (16)$$

This formulation makes it evident that the averaging kernel represents the reduction in the error when the observations are incorporated ($\mathbf{S}$) relative to the error in the a priori ($\mathbf{S}_a$). If the posterior covariance $\mathbf{S}$ is zero, then the retrieval is perfect and the diagonal elements (and hence the DFS) will equal unity. However, if the observations have no sensitivity to the retrieved parameter, then the DFS will be zero. Furthermore, if the prior covariance $\mathbf{S}_a$ is close to zero, then the DFS will approach 0 and if $\mathbf{S}_a$ is "large," then the DFS is maximized (although in this latter case, the retrieval may not converge because the prior would not provide any constraint).

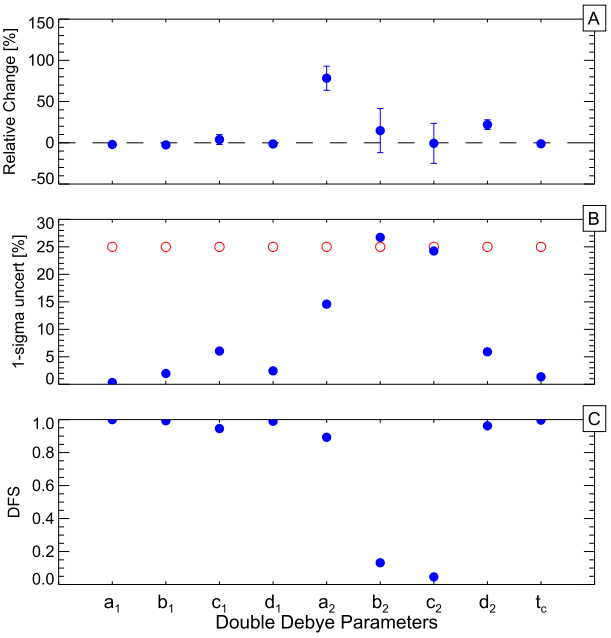

FIG. 1. (a) The relative change in the double-Debye model parameters between the Ellison07 and new TKC model, (b) the uncertainty in the TKC model parameters (blue dots) and the assumed uncertainty in these parameters for the retrieval (red circles), and (c) and the DFS for each of the TKC model parameters.

5. Results

The first step in evaluating the new TKC model is to examine the DFS of the retrieval. The derived DFS for each of the nine TKC coefficients is provided in Fig. 1c and Table 1; the total DFS is 7.0, where the total possible is 9. Increasing the assumed uncertainty in the prior covariance from 25% to 100% increases the DFS by 8%, but it does not change the quality of fit to the data substantially. This analysis demonstrates that the new observations have high information content on seven of the nine coefficients, and thus the resulting uncertainties are small; this suggests that the large 44% and 18% changes in the a_2 and d_2 coefficients between the

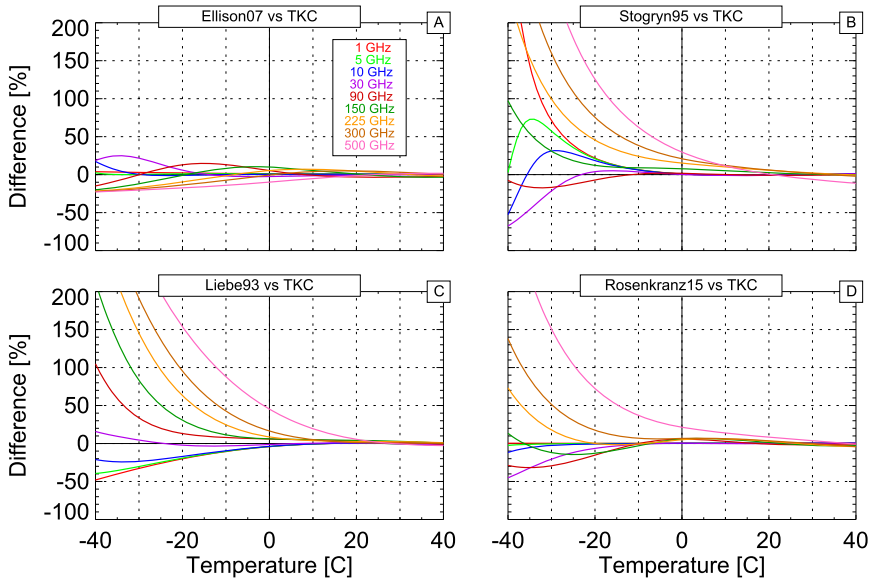

FIG. 2. The change in the liquid water absorption coefficient for the (a) Ellison07, (b) Stogryn95, (c) Liebe93, and (d) Rosenkranz15 models relative to the TKC model, as a function of cloud temperature and frequency.

Ellison07 and TKC models (Table 1) are well supported by the data. However, for two of the coefficients (b_2 and c_2), the observations provide very little information, and thus they are constrained to remain close to the assumed prior (i.e., the Ellison07 coefficients). We will investigate the impact of the uncertainties in the TKC coefficients (i.e., its posterior covariance matrix) in the next section.

The next step in evaluating the new TKC model is to see how it compares to other popular absorption models at different frequencies and temperatures. Figure 2 shows how this model compares against the Ellison07, Stogryn95, Liebe et al. (1993, henceforth Liebe93), and Rosenkranz15 models. The relative difference in the absorption coefficients from the TKC model depends strongly on frequency, and in general increases dramatically for temperatures below −10°C with the largest differences at temperatures below −30°C. The relative differences between the TKC and Ellison07 models are generally small (compared to the Stogryn95, Liebe93, and Rosenkranz15 models), although this might be expected since the TKC model (i) uses the same mathematical formulation as Ellison07 and (ii) the empirical coefficients were constrained to not differ from the Ellison07 by more than 25% (as a 1σ uncertainty). However, there are still some important differences between TKC and Ellison07 (Fig. 2a), such as the 30% difference in α_L at 30 GHz at −30°C, and the 25% difference in α_L at 90 GHz at −20°C. The relative differences with the Stogryn95 model (Fig. 2b) show an interesting "folding" behavior with frequency, with Stogryn95 predicting larger α_L at 1 GHz for supercooled temperatures, better agreement as the frequency increases toward 90 GHz, and then the agreement worsening (again with Stogryn95 predicting α_L larger than TKC) as the frequency increases toward 500 GHz. Contrast this folding behavior with the results comparing Liebe93 and TKC in Fig. 2c, which shows a strictly monotonically increasing difference between the two models as the frequency increases. The best agreement is between TKC and Liebe93 at 30 GHz. Finally, the comparison with Rosenkranz15 (Fig. 2d), which also used the Kneifel14 observations and laboratory data in its formulation, shows some significant differences from TKC, with the 30-, 90-, and 150-GHz absorption from Rosenkranz15 being 10% smaller at −20°C and with frequencies higher than 300 GHz having significantly larger absorption at this temperature. The behavior of the absorption differences between the TKC and Rosenkranz15 models at temperatures colder than −20°C is mixed, with good agreement for frequencies less than 10 GHz, but with a folding behavior for higher frequencies. The differences between the Rosenkranz15 and TKC models may be due to the selection of a subset of the laboratory data used in the fitting (specified in section 2a), the differences in the assumed model formulation, or the method used to fit the absorption model coefficients.

How well does the new model agree with the observations used to fit the coefficients, relative to the

TABLE 2. The RMS difference between the observed and computed permittivity coefficients in different temperature bins (each bin is ±1°C centered upon the indicated temperature). The analysis included all laboratory data between 0.1 and 500 GHz and less than 50°C. Cells with the lowest RMS difference value for each coefficient and temperature range are in bold.

Temp	Model	ε'	ε''	N
0°C	Stogryn95	0.996	0.744	46
	Ellison07	1.099	0.809	
	Rosenkranz15	0.958	**0.690**	
	TKC	**0.942**	0.739	
10°C	Stogryn95	0.914	**0.785**	80
	Ellison07	0.951	0.884	
	Rosenkranz15	0.916	0.850	
	TKC	**0.905**	0.857	
20°C	Stogryn95	0.605	**0.450**	169
	Ellison07	0.588	0.535	
	Rosenkranz15	**0.564**	0.485	
	TKC	0.571	0.490	
40°C	Stogryn95	0.901	0.655	57
	Ellison07	0.893	0.713	
	Rosenkranz15	0.902	0.691	
	TKC	**0.885**	**0.631**	

Stogryn95, Ellison07, and Rosenkranz15 models? Table 2 shows the RMS difference between the laboratory-observed permittivity and the permittivity from the TKC, Rosenkranz15, Ellison07, and Stogryn95 models at four different temperatures. For the lowest temperature bin (0°C), the RMS differences in the permittivity coefficients between the TKC and Rosekranz15 models and observations are virtually identical, and are much lower than the differences between the observations and the other two models. For the higher temperatures (10°, 20°, and 40°C), the RMS differences in the real and imaginary parts of the permittivity are mixed; there is no clear indicator of which model ultimately fits the laboratory data better as not a single model has the lowest RMS difference in both ε' and ε'' simultaneously for any of the three temperature bins. This is shown graphically in Fig. 3, where all four models provide qualitatively the same fit (i.e., are overlapping) to the laboratory data at both 0° and 40°C, although Table 2 does demonstrate that the RMS difference between the observations and models are different.

The only laboratory dataset that spans a significant range of supercooled temperatures is the one collected by Bertolini et al. (1982). This dataset, which consists of 15 measurements at 9.61 GHz, has observations from −18.2° to 32.4°C. Figure 4 shows the modeled and measured real and imaginary parts of the permittivity. Again, the four models are quite similar with the Ellison07, Rosenkranz15, and TKC models almost identical, but at the coldest temperatures the Stogryn95 model underpredicts the value of ε''. However, the RMS

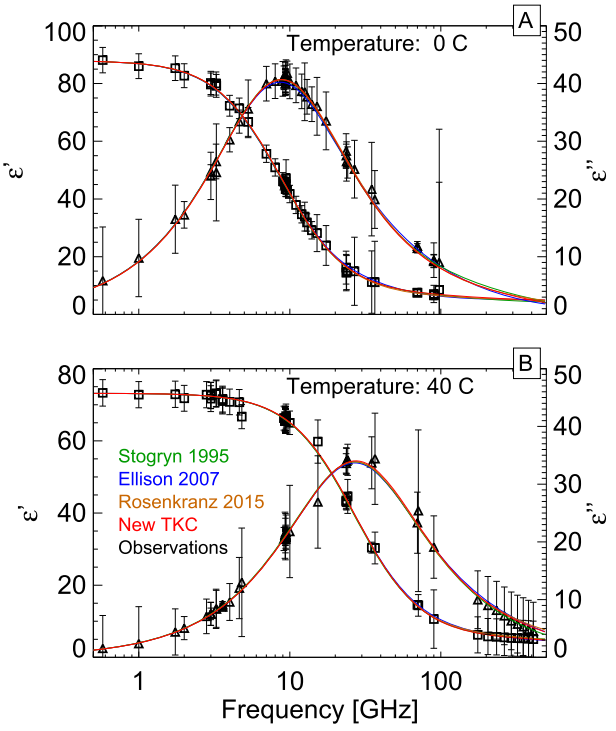

FIG. 3. A comparison of ε' (left axis, squares) and ε'' (right axis, triangles) as a function of frequency between the observations (symbols) and various models (lines) at (a) 0° and (b) 40°C. The observations include all observations from the laboratory data compiled by Ellison07 within 1°C of these two temperatures.

differences between the observations and these models (Table 3) show that the TKC model fits the observations the best in both components, with RMS values markedly less for the TKC model than the Stogryn95, Ellison07, or Rosenkranz15 models.

The comparison of the models relative to the Kneifel14 field observations is shown in Fig. 5. At these supercooled temperatures, the TKC model clearly fits the observations the best over the entire temperature range and at all four frequencies. The other models demonstrate prominent errors, such as grossly overestimating the strength of α_L for all frequencies and supercool temperatures (Liebe93); underestimating α_L at low frequencies and then overestimating at high frequencies, especially for colder temperatures (Stogryn95); or the reverse (Ellison07). The Rosenkranz15 model, which also used these same observations in its formulation, does a poorer job predicting the absorption at 52 GHz relative to both the observations, whereas the TKC model provides a better fit at this frequency. However, the Rosenkranz15 model does fit the mean observations at 31 GHz better than the TKC model, though both are well within the uncertainties of the observations.

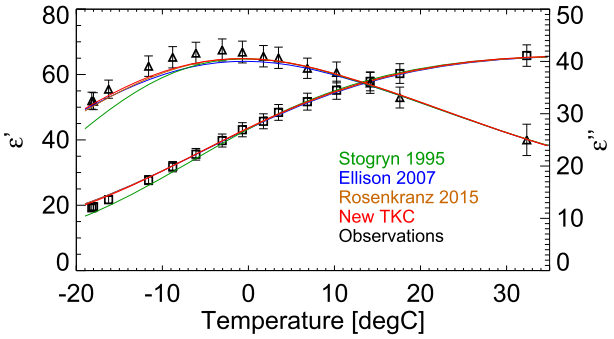

FIG. 4. A comparison of ε' (left axis, squares) and ε'' (right axis, triangles) as a function of temperature using the laboratory observations of Bertolini et al. (1982) at 9.61 GHz.

An advantage of using an optimal estimation framework to derive the TKC model coefficients is that a full error characterization is provided via the posterior covariance matrix **S** [Eq. (12)]. This matrix can be sampled using a Monte Carlo technique to derive other estimates of the fit coefficients that are within the retrieval's uncertainty (Turner and Löhnert 2014). These perturbed coefficients were used to compute α_L at supercooled temperatures, and the interquartile spread of the Monte Carlo sampling is shown as the error bars on the TKC-predicted α_L in Fig. 5. The uncertainties in the α_L predicted by the TKC model (as represented by the interquartile spread) are relatively constant with temperature. There is some slight frequency dependence in the uncertainty of the TKC absorption coefficient, with uncertainties in α_L of 12%, 10%, 12% and 14% at 31, 52, 150, and 255 GHz, respectively.

6. Impact on a LWP retrieval

To evaluate the impact of the new TKC absorption model on a retrieval algorithm, we analyzed all of the microwave radiometer observations at Summit, Greenland, in 2011 using two different liquid water absorption models. These observations were collected as part of the Integrated Characterization of Energy, Clouds, Atmospheric State, and Precipitation over Summit (ICECAPS) campaign (Shupe et al. 2013).

The original LWP retrievals performed on the ICECAPS dataset used the same absorption model used by the U.S. Department of Energy's Atmospheric Radiation Measurement (ARM) Program (Ackerman and Stokes 2003), namely, the absorption model by Liebe91. This model is frequently used in the atmospheric science community. The Liebe91 model has similar liquid water absorption at supercooled temperatures to the Liebe93 model at lower frequencies

TABLE 3. The RMS difference between the observed and computed permittivity coefficients at 9.61 GHz, using the laboratory observations of Bertolini et al. (1982). There were 15 observations in this dataset that ranged from −18.2° to 32.4°C. Cells with the lowest RMS difference value for each coefficient are in bold.

Model	ε'	ε''
Stogryn95	1.116	2.384
Ellison07	0.920	1.564
Rosenkranz15	0.882	1.325
TKC	**0.737**	**1.197**

(i.e., below 30 GHz), but it predicts significantly more absorption than Liebe93 at higher frequencies (dashed vs solid purple lines in Fig. 5). An optimal estimation framework was used to retrieve precipitable water vapor (PWV) and LWP from the MWR observations using the Liebe91 model (Turner et al. 2007; Cadeddu et al. 2013), although only observations at 23.8 and 90.0 GHz were used as input to the retrieval. The forward radiative transfer model, which includes the gaseous absorption models, is the monochromatic radiative transfer model (MonoRTM; Clough et al. 2005).

The retrieved PWV and LWP using the Liebe91 model were used as input into the same radiative transfer model to compute the downwelling brightness temperature (T_b) observed at the other microwave frequencies. The observed minus computed T_b results for 23.8, 31.4, 90, and 150 GHz are shown in Figs. 6a–d, respectively. These results were also aggregated into 5°C bins as a function of LWP (0–25, 25–50, 50–100, and 100–200 g m^{-2}), shown as colored symbols in Fig. 6. The LWP bins demonstrate that the bias in the computed T_b becomes progressively larger as the LWP increases, and that the bias is worse at colder temperatures (i.e., −20°C) than at warmer temperatures. Furthermore, the T_b bias changes sign as the frequency increases, from a positive T_b bias (the radiative transfer model having too little liquid water absorption in the calculation and hence underestimating the downwelling T_b) at 23.8 GHz to a negative T_b bias at 150 GHz.

However, when the TKC model is used in both the retrieval and forward radiative transfer model calculations, the results are much improved (Fig. 7). There is still a slight dependence of the T_b bias on the magnitude of the LWP at 23.8 and 31.4 GHz, but there is little-to-no dependence of the T_b bias on LWP at the higher frequencies. The TKC model somewhat overestimates the liquid water absorption at 23.8 and 31.4 GHz, leading to a negative T_b bias at these frequencies. Further, it slightly underestimates the liquid water absorption at 150 GHz, leading to a very small

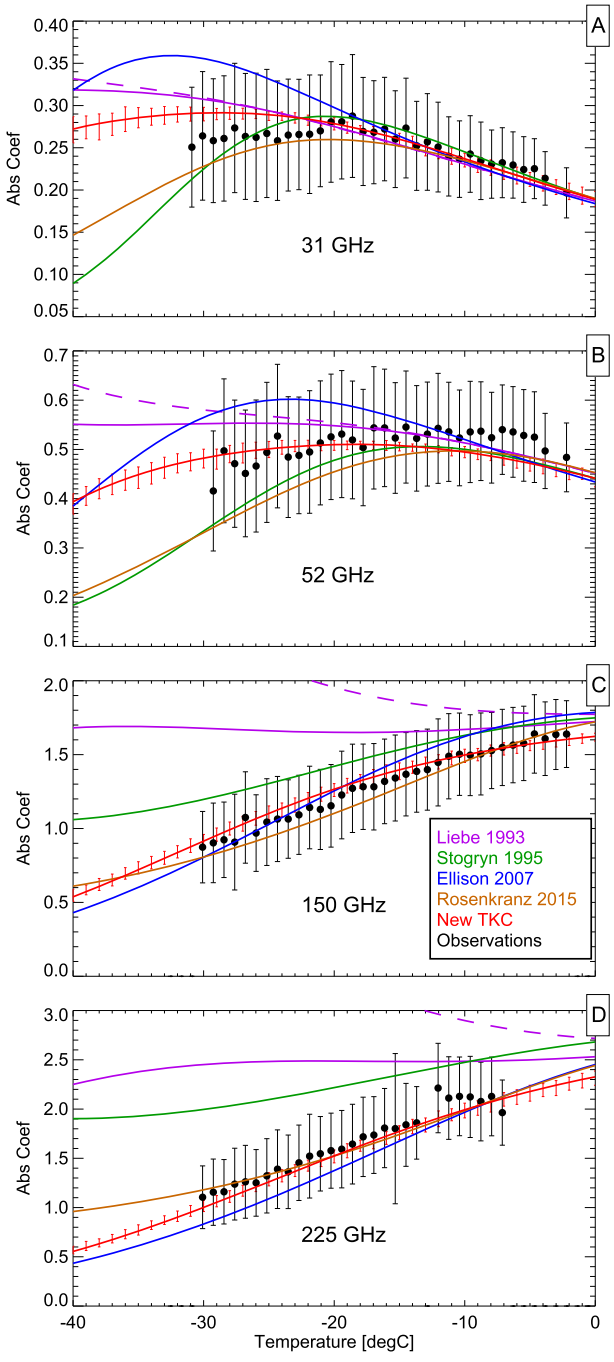

FIG. 5. The modeled liquid water absorption coefficients ($m^2\,kg^{-1}$) for the Liebe91 (dashed purple), Liebe93 (solid purple), Stogryn95 (green), Ellison07 (blue), Rosenkranz15 (brown), and new TKC (red) models, relative to the observations from Kneifel14 at (a) 31, (b) 52, (c) 150, and (d) 225 GHz.

positive T_b bias. Nonetheless, the TKC absorption model provides appreciably better results both as a function of temperature and frequency than the Liebe91 used by the ARM program and many other groups.

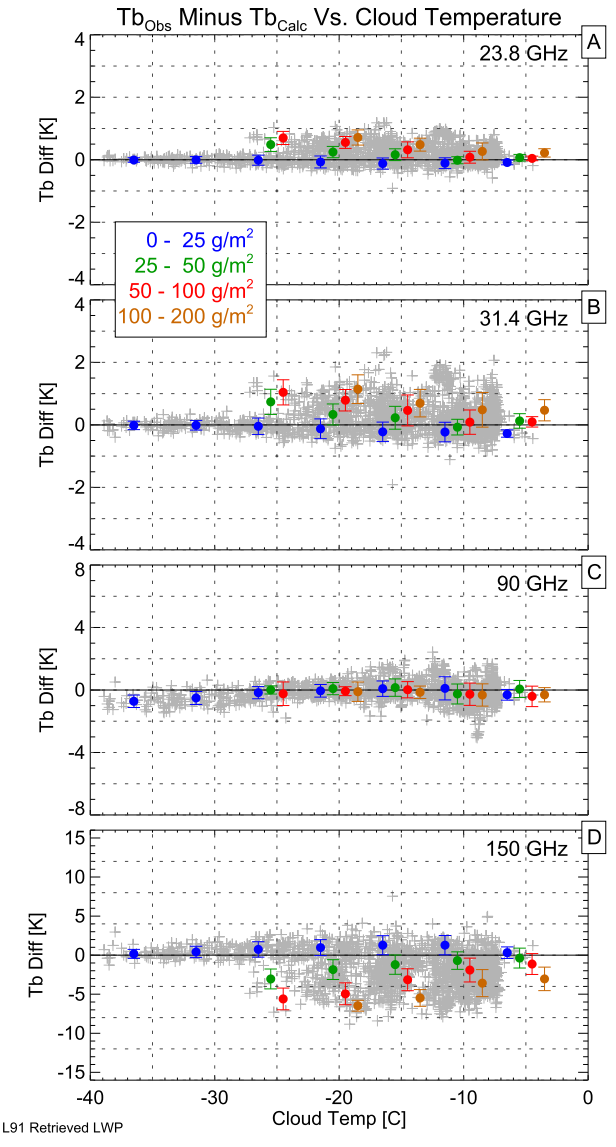

FIG. 6. A comparison of the observed minus computed T_b at (a) 23.8, (b) 31.4, (c) 90.0, and (d) 150 GHz, where the observations were collected at Summit in 2011. The colored symbols (with error bars) represent the mean plus–minus one standard deviation) of the residuals in 5° bins centered at −5°, −10°, −15°, etc., for different LWP bins. The LWP used in the calculation was retrieved from the observations using the Liebe91 model at 90 GHz, and the model used to compute the T_b at each of the four frequencies is also Liebe91.

7. Conclusions

A new liquid water absorption model has been developed for use in the microwave region of the spectrum (defined here as frequencies between 0.5 and 500 GHz). The TKC model uses the same double-Debye framework as suggested by Ellison07. The coefficients of the TKC model were derived using an optimal estimation framework using both laboratory and field observations.

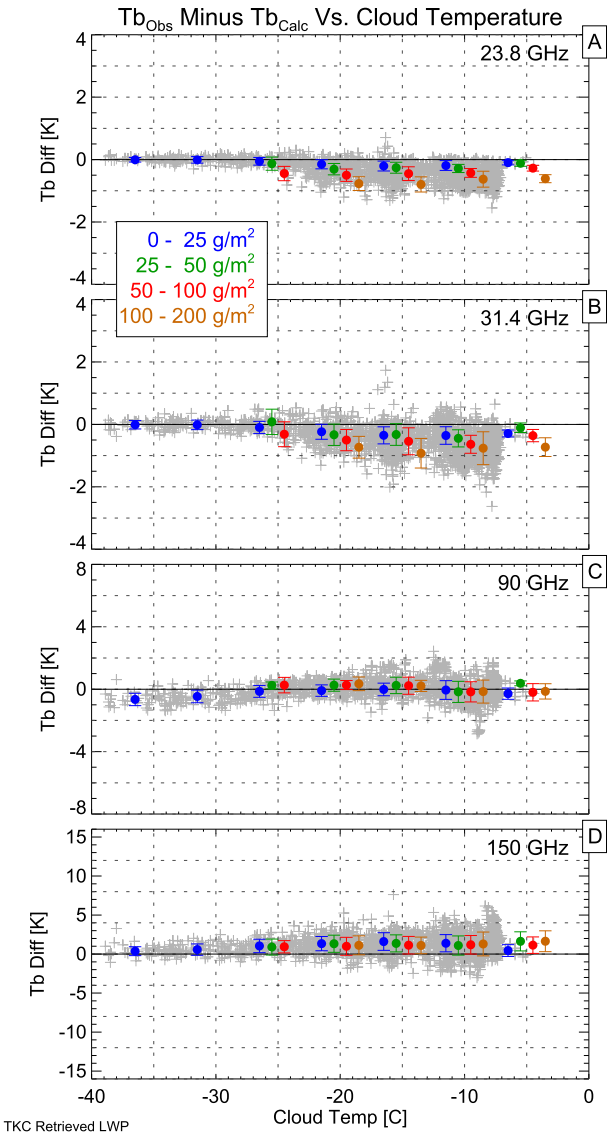

FIG. 7. As in Fig. 6, except that the retrievals and the forward calculation used the TKC model.

This retrieval framework allowed the information content that existed in the observations for each of the nine model coefficients to be determined, and to provide error bars on the predicted α_L values as a function of temperature and frequency.

The retrieval suggests that the observations had little information content for two of the nine empirically derived model coefficients, and thus the uncertainty in these two parameters defaulted to the assumed 25% level. However, the impact of the uncertainty in these two coefficients is small, as the uncertainty in α_L (determined using a Monte Carlo sampling technique) is less than 15% for all temperatures and frequencies between 23 and 225 GHz—and this is true even if larger uncertainties (e.g., 100%) in those two model parameters (namely, the b_2 and c_2 coefficients) were assumed. Furthermore, the TKC model provides the best spectral consistency with observations over the entire range of temperatures (from −35° to 50°C) than any of the other popular models currently used by most atmospheric scientists (e.g., Ellison07, Stogryn95, Liebe93, and Liebe91), and slightly better spectral consistency than a recently published model that used the same input dataset (i.e., Rosenkranz15). Thus, the TKC model provides an improved treatment of cloud liquid water absorption, especially for supercooled temperatures, and is suitable for use in other retrieval algorithms.

The new model was evaluated with the laboratory and field observations used to derive the model, and thus the agreement between the observations and TKC model calculations shown in Figs. 3–5 are really a consistency check and not a validation. New, independent observations are needed, especially at higher frequencies (above 225 GHz) and temperatures below 0°C, to evaluate the adequacy of the TKC model, especially since it differs substantially from the Rosenkranz15 model at those temperatures/frequencies.

There are potentially several impacts that result from this new model. First, by applying an optimal estimation framework in the fitting of the model coefficients, the uncertainty in the modeled absorption can be easily derived, which is useful for both sensitivity studies and data assimilation systems. Second, radiometric observations at frequencies above 150 GHz are being used to derive ice water path information (e.g., Evans et al. 2005), but separating the signal from the emission of supercooled liquid water from the ice scattering requires an accurate estimate of the liquid water absorption. This is particularly true as observations from these higher frequencies are being assimilated into numerical models in an attempt to better specify the ice water path in the simulations (Geer and Baordo 2014). Third, the signal from atmospheric radars can be significantly attenuated by liquid water absorption, and thus improvements in the knowledge of the absorption can reduce the errors in the attenuation correction. The changes in the liquid water absorption between the TKC model and the other absorption models at common radar wavelengths are shown in Table 4. Last, the improved liquid water absorption models yield more accurate retrievals of LWP from spaceborne microwave sensors by removing one source of systematic error.

Acknowledgments. This work was supported by the U.S. Department of Energy's Atmospheric System Research (ASR) program by Grant DE-SC0008830 and by NOAA. The contributions to this study by S. Kneifel

TABLE 4. The difference in liquid water absorption (%) between various models and the TKC model at supercooled temperatures and common radar wavelengths.

		100(model − TKC)/TKC				
Frequency (GHz)	Temp	Rosenkranz15	Ellison07	Stogryn95	Liebe93	Liebe91
3.0 (S band)	−10°C	0.3	1.5	6.4	−10.4	−10.4
	−20°C	0.1	1.8	21.5	−19.8	−19.8
	−30°C	0.0	1.7	66.2	−32.0	−31.9
6.0 (C band)	−10°C	0.1	1.0	6.3	−10.1	−10.1
	−20°C	−0.1	0.6	20.6	−18.9	−18.9
	−30°C	−0.7	−0.3	52.4	−29.2	−29.2
10.0 (X band)	−10°C	−0.2	0.0	6.0	−9.5	−9.5
	−20	−0.7	−1.0	18.5	−17.0	−17.0
	−30	−2.5	0.4	31.1	−23.5	−23.6
35.0 (Ka band)	−10	−0.7	−0.7	3.0	−1.4	−1.6
	−20	−7.6	9.2	0.9	1.0	0.9
	−30	−24.4	22.7	−25.7	7.9	9.1
89.0 (W band)	−10	−0.1	13.1	0.8	7.8	10.0
	−20	−15.2	13.2	−7.2	13.0	20.4
	−30	−29.5	0.2	−17.4	3.0	55.0

were supported by a postdoctoral fellowship from the German Academic Exchange Service (DAAD) and also partly funded by ASR. Effort at Argonne National Laboratory is supported by the U.S. Department of Energy, Office of Science, Office of Biological and Environmental Research, Atmospheric Radiation Measurement Infrastructure Basic Energy Sciences, under Contract DE-AC02-06CH11357. We thank Dušan Zrnić for his helpful comments on a draft of this manuscript. The excellent comments from three anonymous reviewers were also appreciated.

REFERENCES

Ackerman, T. P., and G. M. Stokes, 2003: The Atmospheric Radiation Measurement program. *Phys. Today*, **56**, 38–44, doi:10.1063/1.1554135.

Bertolini, D., M. Cassettari, and G. Salvetti, 1982: The dielectric relaxation time of supercooled water. *J. Chem. Phys.*, **76**, 3285–3290, doi:10.1063/1.443323.

Cadeddu, M. P., and D. D. Turner, 2011: Evaluation of water permittivity models from ground-based observations of cold clouds at frequencies between 23 and 170 GHz. *IEEE Trans. Geosci. Remote Sens.*, **49**, 2999–3008, doi:10.1109/TGRS.2011.2121074.

——, J. C. Liljegren, and D. D. Turner, 2013: The Atmospheric Radiation Measurement (ARM) program network of microwave radiometers: Instruments, data, and retrievals. *Atmos. Meas. Tech.*, **6**, 2359–2372, doi:10.5194/amt-6-2359-2013.

Clough, S. A., M. W. Shephard, E. J. Mlawer, J. S. Delamere, M. J. Iacono, K. Cady-Pereira, S. Boukabara, and P. D. Brown, 2005: Atmospheric radiative transfer modeling: A summary of the AER codes. *J. Quant. Spectrosc. Radiat. Transfer*, **91**, 233–244, doi:10.1016/j.jqsrt.2004.05.058.

Curry, J. A., C. D. Ardeel, and L. Tian, 1990: Liquid water content and precipitation characteristics of stratiform clouds as inferred from satellite microwave measurements. *J. Geophys. Res.*, **95**, 16 659–16 671, doi:10.1029/JD095iD10p16659.

Debye, P., 1929: *Polare Molekeln*. S. Hirzel, 200 pp.

Ellison, W. J., 2007: Permittivity of pure water, at standard atmospheric pressure, over the frequency range 0–25 THz and the temperature range 0–100°C. *J. Phys. Chem. Ref. Data*, **36**, 1, doi:10.1063/1.2360986.

——, K. Lamkaouchi, and J.-M. Moreau, 1996: Water: A dielectric reference. *J. Mol. Liq.*, **68**, 171–279, doi:10.1016/0167-7322(96)00926-9.

Evans, K. F., J. R. Wang, P. E. Racette, G. Heymsfield, and L. Li, 2005: Ice cloud retrievals and analysis with the Compact Scanning Submillimeter Imaging Radiometer and the cloud radar system during CRYSTAL FACE. *J. Appl. Meteor.*, **44**, 839–859, doi:10.1175/JAM2250.1.

Geer, A. J., and F. Baordo, 2014: Improved scattering radiative transfer for frozen hydrometeors at microwave frequencies. *Atmos. Meas. Tech.*, **7**, 1839–1860, doi:10.5194/amt-7-1839-2014.

Greenwald, T. J., 2009: A 2 year comparison of AMSR-E and MODIS cloud liquid water path observations. *Geophys. Res. Lett.*, **36**, L20805, doi:10.1029/2009GL040394.

——, G. L. Stephens, T. H. Vonder Haar, and D. L. Jackson, 1993: A physical retrieval of cloud liquid water over the global oceans using special sensor microwave/imager (SSM/I) observations. *J. Geophys. Res.*, **98**, 18 471–18 488, doi:10.1029/93JD00339.

Hamelin, J., J. B. Mehl, and M. R. Moldover, 1998: The static dielectric constant of liquid water between 274 and 418 K near the saturated vapor pressure. *Int. J. Thermophys.*, **19**, 1359–1380, doi:10.1023/A:1021979401680.

Han, Y., and E. R. Westwater, 2000: Analysis and improvement of tipping calibration for ground-based microwave radiometers. *IEEE Trans. Geosci. Remote Sens.*, **38**, 1260–1276, doi:10.1109/36.843018.

Heng, Z., Y. Fu, G. Liu, R. Zhou, Y. Wang, R. Yuan, J. Guo, and X. Dong, 2014: A study of the distribution of variability of cloud water using ISCCP, SSM/I cloud product, and reanalysis datasets. *J. Climate*, **27**, 3114–3128, doi:10.1175/JCLI-D-13-00031.1.

Hogan, R. J., M. D. Behera, E. J. O'Connor, and A. J. Illingworth, 2004: Estimate of the global distribution of stratiform supercooled liquid water clouds using the LITE lidar. *Geophys. Res. Lett.*, **31**, L05106, doi:10.1029/2003GL018977.

Hu, Y., S. Rodier, K.-M. Xu, W. Sun, J. Huang, B. Lin, P. Zhai, and D. Josset, 2010: Occurrence, liquid water content, and fraction of supercooled water clouds from combined CALIOP/IIR/MODIS measurements. *J. Geophys. Res.*, **115**, D00H34, doi:10.1029/2009JD012384.

Kneifel, S., S. Redl, E. Orlandi, U. Loehnert, M. P. Cadeddu, D. D. Turner, and M.-T. Chen, 2014: Absorption properties of supercooled liquid water between 31 and 225 GHz: Evaluation of absorption models using ground-based observations. *J. Appl. Meteor. Climatol.*, **53**, 1028–1045, doi:10.1175/JAMC-D-13-0214.1.

Liebe, H. J., G. H. Hufford, and T. Manabe, 1991: A model for the complex permittivity of water at frequencies below 1 THz. *Int. J. Infrared Millimeter Waves*, **12**, 659–675, doi:10.1007/BF01008897.

——, ——, and M. G. Cotton, 1993: Propagation modeling of moist air and suspended water/ice particles at frequencies below 1000 GHz. Atmospheric propagation effects through natural and man-made obscurants for visible MM-wave radiation. AGARD Conf. Proc. AGARD-CP-542, NATO, 3-1–3-11.

Lin, B., and W. B. Rossow, 1994: Observations of cloud liquid water path over oceans: Optical and microwave remote sensing methods. *J. Geophys. Res.*, **99**, 20 907–20 927, doi:10.1029/94JD01831.

——, P. Minnis, A. Fan, J. A. Curry, and H. Gerber, 2001: Comparison of cloud liquid water paths derived from in-situ and microwave radiometer data taken during the SHEBA/FIREACE. *Geophys. Res. Lett.*, **28**, 975–978, doi:10.1029/2000GL012386.

Löhnert, U., S. Kneifel, A. Battaglia, M. Hagen, L. Hirsch, and S. Crewell, 2011: A multisensory approach toward a better understanding of snowfall microphysics: The TOSCA project. *Bull. Amer. Meteor. Soc.*, **92**, 613–628, doi:10.1175/2010BAMS2909.1.

Maschwitz, G., U. Löhnert, S. Crewell, T. Rose, and D. D. Turner, 2013: Investigation of ground-based microwave radiometer calibration techniques at 530 hPa. *Atmos. Meas. Tech.*, **6**, 2641–2658, doi:10.5194/amt-6-2641-2013.

Matrosov, S. Y., T. Uttal, and D. A. Hazen, 2004: Evaluation of radar reflectivity–based estimates of water content in stratiform marine clouds. *J. Appl. Meteor.*, **43**, 405–419, doi:10.1175/1520-0450(2004)043<0405:EORREO>2.0.CO;2.

Mätzler, C., P. W. Rosenkranz, and J. Cermak, 2010: Microwave absorption by supercooled clouds and implications for the dielectric properties of water. *J. Geophys. Res.*, **115**, D23208, doi:10.1029/2010JD014283.

Meissner, T., and F. J. Wentz, 2004: The complex dielectric constant of pure and sea water from microwave satellite observations. *IEEE Trans. Geosci. Remote Sens.*, **42**, 1836–1849, doi:10.1109/TGRS.2004.831888.

Minnis, P., and Coauthors, 1995: Cloud optical property retrieval (subsystem 4.3). Cloud analyses and determination of improved top of atmosphere fluxes (subsystem 4), Vol. III, Clouds and the Earth's Radiant Energy System (CERES) algorithm theoretical basis document, NASA Reference Publ. 1376, 135–176.

O'Dell, C. W., F. J. Wentz, and R. Bennartz, 2008: Cloud liquid water path from satellite-based passive microwave observations: A new climatology over the global oceans. *J. Climate*, **21**, 1721–1739, doi:10.1175/2007JCLI1958.1.

Petty, G. W., and K. B. Katsaros, 1992: The response of the SMM/I to the marine environment. Part I: An analytic model for the atmospheric component of observed brightness temperature. *J. Atmos. Oceanic Technol.*, **9**, 746–761, doi:10.1175/1520-0426(1992)009<0746:TROTST>2.0.CO;2.

Rodgers, C. D., 2000: *Inverse Methods for Atmospheric Sounding: Theory and Practice*. Series on Atmospheric, Oceanic, and Planetary Physics, Vol. 2, World Scientific, 238 pp.

Rose, T., S. Crewell, U. Löhnert, and C. Simmer, 2005: A network suitable microwave radiometer for operational monitoring of the cloudy atmosphere. *Atmos. Res.*, **75**, 183–200, doi:10.1016/j.atmosres.2004.12.005.

Rosenkranz, P. W., 2015: A model for the complex dielectric constant of supercooled liquid water at microwave frequencies. *IEEE Trans. Geosci. Remote Sens.*, **53**, 1387–1393, doi:10.1109/TGRS.2014.2339015.

Shupe, M. D., and Coauthors, 2013: High and dry: New observations of tropospheric and cloud properties above the Greenland Ice Sheet. *Bull. Amer. Meteor. Soc.*, **94**, 169–186, doi:10.1175/BAMS-D-11-00249.1.

Stogryn, A. P., H. T. Bull, K. Rubayi, and S. Iravanchy, 1995: The microwave permittivity of sea and fresh water. GenCorp Aerojet Rep., 24 pp.

Tereschin, S., 1889: Die Dielectricitätsconstanten einiger organischer Flüssigkeiten. *Ann. Phys.*, **272**, 792–804, doi:10.1002/andp.18892720404.

Turner, D. D., 2007: Improved ground-based liquid water path retrievals using a combined infrared and microwave approach. *J. Geophys. Res.*, **112**, D15204, doi:10.1029/2007JD008530.

——, 2015: Dataset used to improve liquid water absorption models in the microwave. Atmospheric Radiation Measurement (ARM) Climate Research Facility Data Archive, accessed 14 December 2015, doi:10.5439/1228766.

——, and U. Löhnert, 2014: Information content and uncertainties in thermodynamic profiles and liquid cloud properties retrieved from the ground-based Atmospheric Emitted Radiance Interferometer (AERI). *J. Appl. Meteor. Climatol.*, **53**, 752–771, doi:10.1175/JAMC-D-13-0126.1.

——, S. A. Clough, J. C. Liljegren, E. E. Clothiaux, K. Cady-Pereira, and K. L. Gaustad, 2007: Retrieving liquid water path and precipitable water vapor from Atmospheric Radiation Measurement (ARM) microwave radiometers. *IEEE Trans. Geosci. Remote Sens.*, **45**, 3680–2690, doi:10.1109/TGRS.2007.903703.

Westwater, E. R., Y. Han, M. D. Shupe, and S. Y. Matrosov, 2001: Analysis of cloud liquid and precipitable water vapor retrievals from microwave radiometers during the Surface Heat Budget of the Arctic Ocean project. *J. Geophys. Res.*, **106**, 32 019–32 030, doi:10.1029/2000JD000055.

Wulfmeyer, V., and Coauthors, 2008: The Convective and Orographically Induced Precipitation Study: A research and development project of the World Weather Research Program for improving quantitative precipitation forecasting in low-mountain regions. *Bull. Amer. Meteor. Soc.*, **89**, 1477–1486, doi:10.1175/2008BAMS2367.1.